DFT calculations of the structural, elastic, and electronic properties of (Bi1-xFex)2Te3 chalcogenides

To cite this article before publication: Eugenia Paola Arévalo López *et al* 2024 *Phys. Scr.* in press https://doi.org/10.1088/1402-4896/ad1c24

DFT calculations of the structural, elastic, and electronic properties of $(Bi_{1-x}Fe_x)_2Te_3$ chalcogenides

E. P. Arévalo-López[1], J. Pilo[1], J. L. Rosas-Huerta[2], J. E. Antonio[1], H. Muñoz[3], A. Benitez-Rico[5], R. Escamilla[1,4] and M. Romero[1*]

[1] Facultad de Ciencias, Universidad Nacional Autónoma de México, Apartado Postal 70-399, México CDMX, 04510, México.

[2] Unité de Catalyse et Chimie du Solide (UCCS) - UMR CNRS 8181, Université de Lille - Centrale Lille, ENSCL, Lille, F-59000, France.

[3] Escuela Superior de Ingeniería Mecánica y Eléctrica-Culhuacán, Instituto Politécnico Nacional, Av. Santa Ana 1000, México CDMX, 04440, México

[4] Instituto de Investigaciones en Materiales, Universidad Nacional Autónoma de México, Apartado Postal 70-360, México CDMX, 04510, México.

[5] Vicerrectoría de Investigación, Universidad La Salle México, Benjamín Franklin 45, Colonia Condesa, Cuauhtémoc, 06140 Ciudad de México, CDMX.

*Corresponding Author e-mail: mromero@ciencias.unam.mx

Abstract

The crystal structure and elastic and electronic properties of $(Bi_{1-x}Fe_x)_2Te_3$ were studied by first-principles calculations within the Density Functional Theory (DFT) scheme. We found that at zero GPa, the lattice parameters for Bi_2Te_3 are in good agreement with the available experimental and theoretical data. As Fe replaces bismuth, the lattice parameter *a* increases while *c* decreases, changing the unit cell volume. According to Born's structural stability criterion, the system is mechanically stable. Poisson's ratio suggests a change from brittle to ductile behavior for $(Bi_{1-x}Fe_x)_2Te_3$ as iron increases. Also, Poisson's ratio indicates that there is an ionic-covalent bond for x = 0.00 and behave as a metal as iron content increases. Vickers

hardness decreases its value as Fe is introduced in the compound. Band structure calculations show that the results with spin orbit coupling (SOC) and without SOC are in good agreement with the experimental results. With SOC, a direct band gap at the Γ point is obtained with Eg = 0.138 eV concerning the 0.226 eV obtained without SOC. An evident modification of crystal structure in $(Bi_{1-x}Fe_x)_2Te_3$ shows a consistent trend, indicating a significant impact of iron incorporation on the structural properties. The electronic properties show a significant transformation with the introduction of iron, Bi_2Te_3 is characterized by a band gap, through iron doping the electronic structure shows a complete elimination of the band gap, marking a transition from semiconductor towards a conductor-like behavior. Density of states analysis provided insight into these changes, illustrating a modulation of electronic properties dependent on iron content.

Keywords: Bismuth chalcogenides, topological insulators, elastic properties, electronic properties, DFT.

1. Introduction

Bi_2Te_3 is a compound with interesting physical properties used for decades as a thermoelectric material. In recent years it has been reported as a topological insulator, which means it has unique electronic properties that allow it to conduct on its surface but not through the bulk [1] [2] [3]. These properties make the compound a potential candidate in electronic devices such as thermoelectric generators and quantum computing [4] [5] [6] [7].

The mechanical properties of Bi_2Te_3 have been studied extensively [8] [9] [10] [11] [12], it shows a relatively high Young's modulus of ~71 GPa [13], which means it is a stiff and brittle material [14] [15] [16]. Regarding the thermoelectric properties, Zhu *et al*. [17] have reported excellent results in commercial Bi_2Te_3, the electrical conductivity (σ) is about 925 S/cm at 400 K, while the Seebeck coefficient (S) is -215 mV/K at the same temperature, at 400 K bismuth telluride shows a thermal conductivity (κ) of ~1.5 W/mK, these parameters give a figure of merit (ZT) of ~1.16 at 400 K [17], which is calculated as: $ZT = \frac{S^2\sigma}{\kappa}T$ [18]. Finally, it shows good stability under high-temperature and pressure making the compound suitable for high-temperature applications.

Bi_2Te_3 crystallizes in a rhombohedral structure with space group $R\bar{3}m$ (No. 166), Figure 1(a). In this structure, layers of bismuth and tellurium are intercalated in the form Te1-Bi-Te2-Bi-Te1, where 1 and 2 correspond to different Wyckoff positions, Bi corresponds to the Wyckoff position 6c (0, 0, 0.40), Te1 to 3a (0, 0, 0), and Te2 to 6c (0, 0, 0.21), this array is often known as a quintuple layer and is marked in a green box in the hexagonal unit cell shown in Figure 1(a). When a dopant is introduced into Bi_2Te_3, it enters the structure in different ways [19] [20] [21] [22] [23]. The first case is when the dopant substitutes Bi atoms in the structure, Figure 1(b), usually the ionic radii of these substituents are smaller than that of bismuth, then this could cause a shrink of the crystal structure, giving smaller lattice parameters and volume than those of Bi_2Te_3. The second case is when the dopant is intercalated between bismuth and tellurium layers inside the quintuple layer. Finally, a third case could be considered when the dopant is intercalated in between Te1 and another Te1 from different Te1-Bi-Te2-Bi-Te1 arrays, in which the Wyckoff position of the dopant corresponds to 3b (0, 0, ½) [24] [25].

The last two cases increase the lattice parameter c, which generates an increase in the unit cell volume compared to Bi_2Te_3 [26] [27].

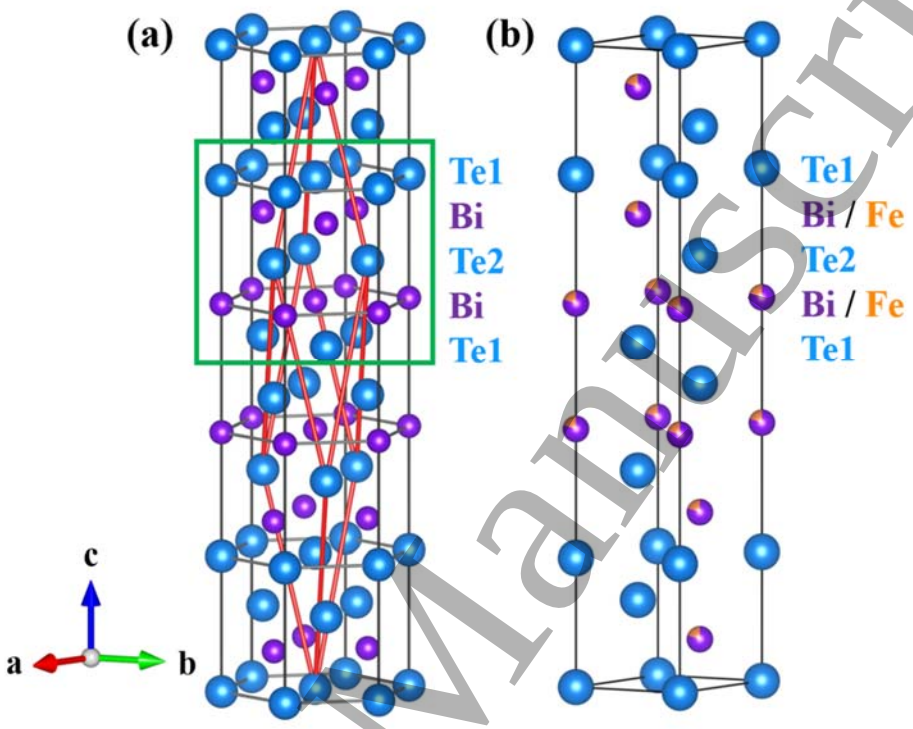

Figure 1. (a) Schematic representation of Bi_2Te_3 with space group R-3m (No. 166) in hexagonal crystal structure with the rhombohedral unit cell in red. The green box indicates the quintuple layer array in the structure. (b) Doping Bi_2Te_3 with Fe in Bi sites, $(Bi_{1-x}Fe_x)_2Te_3$. The structures were modelled with VESTA Software [28].

Doping Bi_2Te_3 with different metals has been shown to improve the figure of merit and its mechanical properties, including hardness. Lou *et al*. reported that doping with 0.25wt % Na, the hardness increased by 23 %, while Young's modulus increased by 21 % from the doped polycrystalline Bi_2Te_3 [29]. Regarding the figure of merit, the system reported by Lou *et al*. increases by ~70 % around 300 K, reaching a maximum ZT ≈ 1.03 [29]. Vaney *et al*. reported

positive changes in thermopower and a higher power factor due to magnetic interactions of Cr substitution in Bi_2Te_3, which decreases the thermal conductivity [30]. Therefore, by doping Bi_2Te_3 with different metals, the mechanical and thermoelectric properties can be improved to increase the field of application of this thermoelectric system.

Fe is an element that has been used as a dopant in bismuth chalcogenides with the purpose of studying and modifying the magnetic properties in Bi_2Se_3 and Bi_2Te_3 [31] [32] [33] [34] [35] [36]. Introducing magnetic atoms into bismuth chalcogenides can modulate the Fermi level in the exchange gap resulting in a quantum Hall effect at zero magnetic field [37], known as Quantum Anomalous Hall Effect [38] [39] [40], with other interesting effects, as the topological magnetoelectric effect [37], magneto-optical effect [41], allowing a new approach to develop electronic devices with a dissipation less edge transport in low-power electronic circuits to be applied in low-energy consumption spintronics and topological quantum computing [42]. However, the effect of Fe-doped on Bi_2Te_3 for the study of mechanical and elastic properties has not been investigated.

Furthermore, experimentally it is difficult to achieve large amounts of dopants into bismuth chalcogenides, in $Ni_xBi_{2-x}Se_3$ x = 0.03, 0.05, 0.07 and 0.1 [43], reports on $(Bi_{1-x}Fe_x)_2Se_3$ with no more than 10 at% of Fe [44], single crystals of $M_xBi_2Te_3$, where M = Fe, Ru, and Os, have been reported with nominal x values between 0.00 and 0.06 [45], and for different alkali earth metals (AE) as dopants $AE_{0.01}Bi_{1.99}Te_3$ where AE = Mg, Ca, Sr, Ba and $Mg_xBi_{2-x}Te_3$ with x = 0. 0.005, 0.01, 0.015 [46]. Moreover, recently Kander *et al*. [47] published an experimental article on $Fe_xBi_{2-x}Se_3$ with x = 0.1 and 0.4, at low concentration of Fe in Bi_2Se_3 the dopant replaces Bi; whereas, at high concentration (x = 0.4) both substitution in Bi sites and intercalation in the host occurs [47]. Specifically, for Bi_2Te_3 doped with Fe, small amounts

of the dopant ($x \leq 0.2$) generate magnetic properties at low temperature, weak ferromagnetism at $T_C = 14$ K [48], higher concentrations of the dopant (8 %, $x = 0.4$) indicate that the dopant enters the structure in Bi sites and with interstitial incorporation of Fe [40]. Therefore, in this work a systematic study of the crystalline structure and mechanical, electronic properties of Bi_2Te_3 with Fe as dopant in Bi sites with $x = 0.0 - 0.2$ is performed by first-principles calculations based on the density functional theory (DFT).

2. Calculation Method

Geometry optimization, elastic constants, band structure, and the total and partial density of states were calculated using Cambridge Serial Total Energy Package (CASTEP) code [49] [50] based on DFT [51] with the Projector Augmented Wave (PAW) method [52] [53] and the Generalized Gradient Approximation (GGA); PBEsol functional [54] [55] with an ultrasoft pseudopotential was used for the electronic exchange-correlation energy. A basis set of plane waves were defined at 400 eV of kinetic energy cut-off. A rhombohedral cell along the z-axis can be created from hexagonal close-packed atomic layers, as shown in Figure 1 (a). The rhombohedral structure, shown in red, can be represented by a hexagonal, in this work the calculations were performed with the hexagonal one. For the geometry optimization in all the compounds, the experimental constants of the hexagonal lattice for Bi_2Te_3 considered initially were $a = 4.386$ Å and $c = 30.497$ Å [56], the atomic positions were optimized until the maximum atomic force was less than 0.01 eV/Å and 5×10^{-4} Å for the maximum atomic displacement. The self-consistent field (SCF) tolerance was set to 5×10^{-7} eV/atom [57] [58]. The highest stress tolerance amplitude in these calculations was 0.02 GPa. A grid of 7×7×1 k-points of the Brillouin zone on the Monkhorst-Pack scheme [59]

was employed. We implemented the virtual crystal approximation (VCA) [60] to simulate the substitution of Bi by Fe atoms in $(Bi_{1-x}Fe_x)_2Te_3$ with x = 0.05 - 0.20, as depicted in Figure 1 (b). To determine elastic constants, homogeneous deformations were applied to the three coordinate axes, and the resulting stress was calculated concerning the optimization of the crystal structure. Broyden-Fletcher-Goldfarb-Shanno (BFGS) minimization scheme was used for geometry optimization [61]. For bismuth, tellurium, and iron atoms, the $6s^26p^3$, $5s^25p^4$, and $3d^64s^2$ orbitals were considered valence electrons, respectively. In contrast, the presence of tightly bound core electrons was represented by a norm-conserving Vanderbilt-type pseudopotential [62].

3. Results and discussion

3.1 Crystal structure

The crystal structure of Bi_2Te_3 is shown in Figure 1, which is rhombohedral with space group $R\bar{3}m$ (No. 166). The optimized lattice parameters *a* and *c* and the unit cell volume as a function of iron content *x* are shown in Figure 2. Table 1 shows the lattice parameters *a* and *c*, unit cell volume, *c/a* ratio, Bi/Fe-Te1, and Bi/Fe-Te2 bond lengths, as well as the bond angles Bi/Fe-Te1-Bi/Fe and Te2-Bi/Fe-Te1 in the system. For x= 0.0, lattice parameters *a* and *c* differ by 0.02 % and 1.20 % from those experimentally reported [56]. Lattice parameter *a* increases as Fe content increases; the increase in the parameter *a* might be caused by the strong interaction between Bi/Fe atoms in the *a-b* plane, the electronic repulsion must be compensated and this causes a decrease in the z-axis and increases the parameter *a*, the maximum value is reached when x = 0.20, showing an increase of 4.7 %. We observe a decrease in the *c* lattice parameter as more iron is introduced into the compound.

Consequently, the unit cell volume decreases up to 0.8 % as iron is introduced (x = 0.20). From Table 1, Bi/Fe-Te1 bond lengths do not change as Fe replaces Bi in the structure. However, in Bi/Fe-Te2 bond length, as the amount of dopant increases, the distance also increases. Additionally, the bond angles, formed by Bi/Fe-Te1-Bi/Fe and Te2-Bi/Fe-Te1, are shown; in both cases the angle decreases as the Fe content in the system increases. Due to the difference in ionic radii between Bi (0.96 Å) and Fe (0.58 Å) [63], *c* parameter decreases as iron is introduced into Bi sites and, consequently, the bond angles Bi/Fe-Te1-Bi/Fe and Te2-Bi/Fe-Te1 decrease, giving rise to electronic repulsion that is compensated by an elongation in the *a*-*b* plane, which is observed in the increase of the lattice parameter *a* and the Bi/Fe-Te2 bond distance. Moreover, this behavior has been observed in experimental and theoretical reports in similar systems [48] [64] [65] [66].

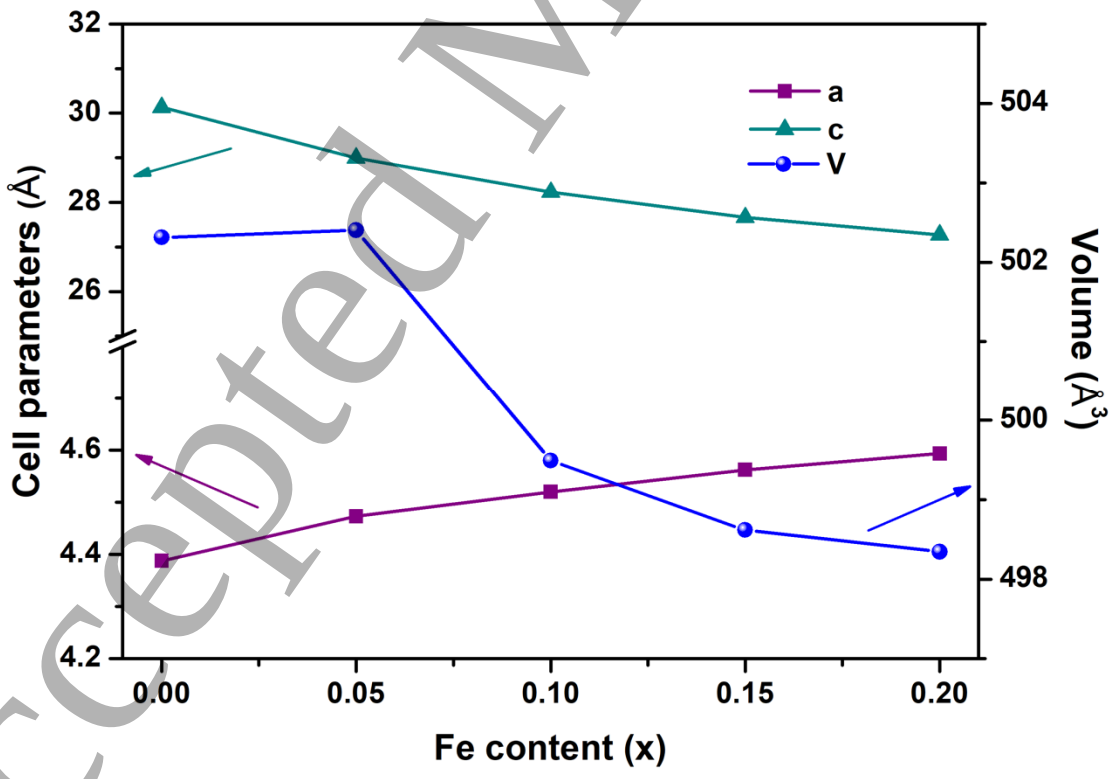

Figure 2. Optimized lattice parameters and unit cell volume as a function of the content of Fe in $(Bi_{1-x}Fe_x)_2Te_3$ compounds.

Table 1. Lattice parameters *a* and *c*, unit cell volume, *c/a* ratio, Bi/Fe-Te1 and Bi/Fe-Te2 bond lengths, and bond angles between Bi/Fe-Te1-Bi/Fe and Te2-Bi/Fe-Te1 for $(Bi_{1-x}Fe_x)_2Te_3$.

Fe content (*x*)	*a* (Å)	*c* (Å)	Volume (Å^3)	*c/a*	Bi/Fe-Te1 (Å)	Bi/Fe-Te2 (Å)	Bi/Fe-Te1-Bi/Fe (°)	Te2-Bi/Fe-Te1 (°)
0.00	**4.387**	**30.131**	**502.32**	**6.87**	**3.234**	**3.069**	**94.561**	**91.584**
0.05	**4.473**	**28.995**	**502.40**	**6.48**	**3.241**	**3.096**	**92.711**	**90.046**
0.10	**4.520**	**28.227**	**499.49**	**6.24**	**3.240**	**3.127**	**91.537**	**89.441**
0.15	**4.562**	**27.662**	**498.62**	**6.06**	**3.239**	**3.156**	**90.462**	**88.919**
0.20	**4.593**	**27.274**	**498.34**	**5.94**	**3.238**	**3.182**	**89.640**	**88.619**
Ref. [56] [a]	**4.386**	**30.497**						
Ref. [67] [b]	**4.383**	**30.487**						
Ref. [68] [c]	**4.466**	**30.909**						
Ref. [69] [d]	**4.375**	**30.193**						

[a]Experimental, [b,c]Theoretical (GGA-PBE), [d]Theoretical (GGA-PBEsol). The reports mentioned above are for x = 0.00.

The formation energy was calculated for each system using the following expression [70]:

$$E_f = \frac{1}{M}(E_{sis\ bulk} - n_{Bi}E_{Bi\ bulk} - n_{Fe}E_{Fe\ bulk} - n_{Te}E_{Te\ bulk}) \quad (1)$$

where, M is the total number of atoms in the system, $E_{sis\ bulk}$ is the bulk system energy, $E_{Bi\ bulk}$, $E_{Fe\ bulk}$, and $E_{Te\ bulk}$ correspond to Bi, Fe and Te energy in bulk respectively, and n_{Bi}, n_{Fe}, and n_{Te} are the number of Bi, Fe and Te atoms in the system, respectively. Table 2 shows the total energy and the calculated formation energies, E_{tot} increases as the amount of dopant increases. However, when calculating the formation energy according to (1), all systems show negative energy, which becomes more negative as Fe content increases suggesting that

the studied compounds are thermodynamically stable. Experimentally, Bi_2Te_3 single crystals have been synthesized by the solid-state reaction method inside a vacuum-sealed quartz ampoule [71] [72] [73]. Inside the ampoule at ~ 900°C it might exist a vapor pressure due to the low boiling points of the elements involved, producing the stabilization of the system. Nevertheless, in this work the systems are not subjected to any external pressure, so at P = 0 GPa and T = 0 K the formation energies are negative. The material's response to structural changes by Fe doping, positions it as a promising candidate for advanced technologies. The correlation between structural adaptability and thermodynamic stability in $(Bi_{1-x}Fe_x)_2Te_3$ projects a promising scenario, indicating some notions for future applications in electronics and thermoelectric devices.

Table 2. Total energy (E_{tot}) and formation energy (E_f) for $(Bi_{1-x}Fe_x)_2Te_3$.

Fe content (x)	E_{tot} (eV)	E_f (eV/atom)
0.00	**-7481.666**	**-0.888**
0.05	**-7515.173**	**-1.458**
0.10	**-7556.857**	**-1.992**
0.15	**-7604.640**	**-2.498**
0.20	**-7657.556**	**-2.982**
x = 0.0 [a]		**-0.237**
x = 0.0 [b]		**-0.509**
$(Bi_{0.96}In_{0.04})_2Te_3$ [c]		**-0.970**
$(Bi_{0.96}Po_{0.04})_2Te_3$ [c]		**-0.850**

[a] Ref. [74], [b] Ref. [75], [c] Ref. [76].

3.2 Mechanical properties

The mechanical properties of $(Bi_{1-x}Fe_x)_2Te_3$ compounds with the rhombohedral (I) structure and Laue class $\bar{3}m$ [77] were calculated the six independent elastic constants (C_{ij}), which are

C_{11}, C_{12}, C_{13}, C_{14}, C_{33}, and C_{44}, and one dependent C_{66} [77]. Table 3 shows the calculated values, where $C_{66} = (C_{11} - C_{12})/2$. Considering Born's criteria, four necessary and sufficient conditions must be satisfied: $C_{11} > |C_{12}|$, $C_{44} > 0$, $C_{13}^2 < \frac{1}{2}C_{33}(C_{11} + C_{12})$, and $C_{14}^2 < \frac{1}{2}C_{44}(C_{11} - C_{12}) \equiv C_{44}C_{66}$ [77] [78]. The calculated elastic constants satisfy these conditions, therefore, $(Bi_{1-x}Fe_x)_2Te_3$ compounds with x = 0.05 - 0.20 are mechanically stable.

The C_{11} and C_{33} elastic constants measure the specific direction in which there is linear compression resistance; C_{11} indicates this resistance in the *a*-direction and C_{33} in the *c*-direction. From Table 3, the lower calculated values of C_{33} with respect to C_{11} ; suggests that the crystal is more compressible along the c-direction than along the a-direction. This behavior is reflected in the lattice parameters; the resistance to linear compression is stronger along the lattice parameter *a* than in lattice parameter *c*. As iron is introduced into the compound the lattice parameter *c* decreases; for x = 0.20 *c* parameter reduces by ~9.5% while *a* parameter increases by ~4.7 %, with respect to x = 0.00. In addition, the resistance in the *a* direction decreases, on the contrary in the *c* direction it increases; however the axial resistance to these planes increases, which could be the effect of the Fe *p* orbitals, and *a* consequence is the decrease in the shear force for both directions.

Table 3. Elastic constants (C_{ij}), calculated with DFT of $(Bi_{1-x}Fe_x)_2Te_3$ compounds.

Fe content (*x*)	C_{11} (GPa)	C_{12} (GPa)	C_{13} (GPa)	C_{14} (GPa)	C_{33} (GPa)	C_{44} (GPa)	C_{66} (GPa)
0.00	**76.98**	**17.86**	**25.67**	**19.07**	**46.92**	**35.64**	**29.56**
0.05	**74.64**	**28.42**	**32.19**	**22.59**	**51.99**	**42.11**	**23.11**
0.10	**70.16**	**39.00**	**39.20**	**17.71**	**64.13**	**39.00**	**15.58**
0.15	**71.67**	**41.65**	**45.87**	**15.20**	**64.66**	**26.97**	**15.01**
0.20	**67.48**	**55.57**	**47.77**	**5.29**	**55.93**	**15.75**	**5.95**

Ref. [79] **Exp.**	**74.4**	**21.7**	**29.2**	**15.4**	**51.6**	**31.4**	**26.2**
Ref. [78] **Teo.**	**75.3**	**23.6**	**25.1**	**---**	**49.3**	**23.5**	**25.8**
Ref. [14] **Teo.**	**73.8**	**16.3**	**30.6**	**---**	**54.3**	**30.4**	**28.7**
Ref. [80] **Teo.**	**72.1**	**12.7**	**28.3**	**---**	**50.4**	**28.8**	**---**
Ref. [13] **Teo.**	**82.8**	**20.8**	**36.1**	**---**	**60.4**	**40.1**	**31.0**

Refs. for x = 0.00

The elastic moduli were obtained from the calculated elastic constants using the Voigt-Reuss-Hill approximation [81] [82] [83]. Hill's elastic moduli are obtained from an arithmetic average of the Voigt and Reuss moduli [84]. Table 4 shows the bulk (B) and shear (G) moduli as a function of iron content. Bulk modulus indicates how resistant to compression the material is. In Figure 3(a) we observe that as iron increases B increases, this suggests that the material is becoming less compressible; an increase in B indicates greater resistance to volumetric deformation, in this compound a rise of ~ 46% is observed from x = 0.00 to x = 0.20. The behavior mentioned above is reflected in the volume cell value reduction as iron is introduced. The shear modulus is related to the stiffness of the material; in this system as the iron content increases, the material becomes less resistant to axial deformation corresponding to a decrease of ~ 66% from Bi_2Te_3 in comparison with $(Bi_{1-x}Fe_x)_2Te_3$ when x = 0.20, as shown in Figure 3(a).

The mechanical properties such as Pugh's criterion (G/B), Poisson's ratio (v), Young modulus (E), Vickers hardness (H_v), average sound velocity (v_m), and Debye temperature (θ_D) (elastic contribution) for $(Bi_{1-x}Fe_x)_2Te_3$ compounds are shown in Table 4. Through Pugh's criterion, we can elucidate if the material is brittle ($G/B > 0.57$) or ductile ($G/B < 0.57$) [85]. Therefore, from Table 4 we observe that for x = 0.00, we have a brittle material. This result is in good agreement with other theoretical reports [79] [80], as we introduce iron

the material becomes ductile, shown in Figure 3(b). From x = 0.00 to 0.20, a decrease of ~ 77% in Pugh´s criterion is observed. Another parameter associated with ductility is Poisson's ratio (v), which is calculated with B and G moduli considering Hill's approximation as: $\nu = \frac{3B-2G}{6B+2G}$ [86]. A material is ductile when ν is higher than 0.26, otherwise it is brittle; when x = 0.00, ν has a value of 0.233, indicating a brittle material. When the iron is substituted in bismuth sites this value changes to 0.285 and higher, suggesting a transition to a ductile material. Typically, Poisson's ratio for metals is around 0.33; for the ionic-covalent crystal, it is between 0.20 and 0.30, therefore the material studied here has a transition from ionic-covalent crystal to metallic crystal due to the interaction of Fe orbitals. Poisson's ratio as a function of iron content is shown in Figure 3(b); we observe that v increases ~ 84%, from x = 0.00 to x = 0.20, as iron increases the compound tend to be more ductile. Therefore, both G/B and v indicate a brittle to ductile transition in these compounds.

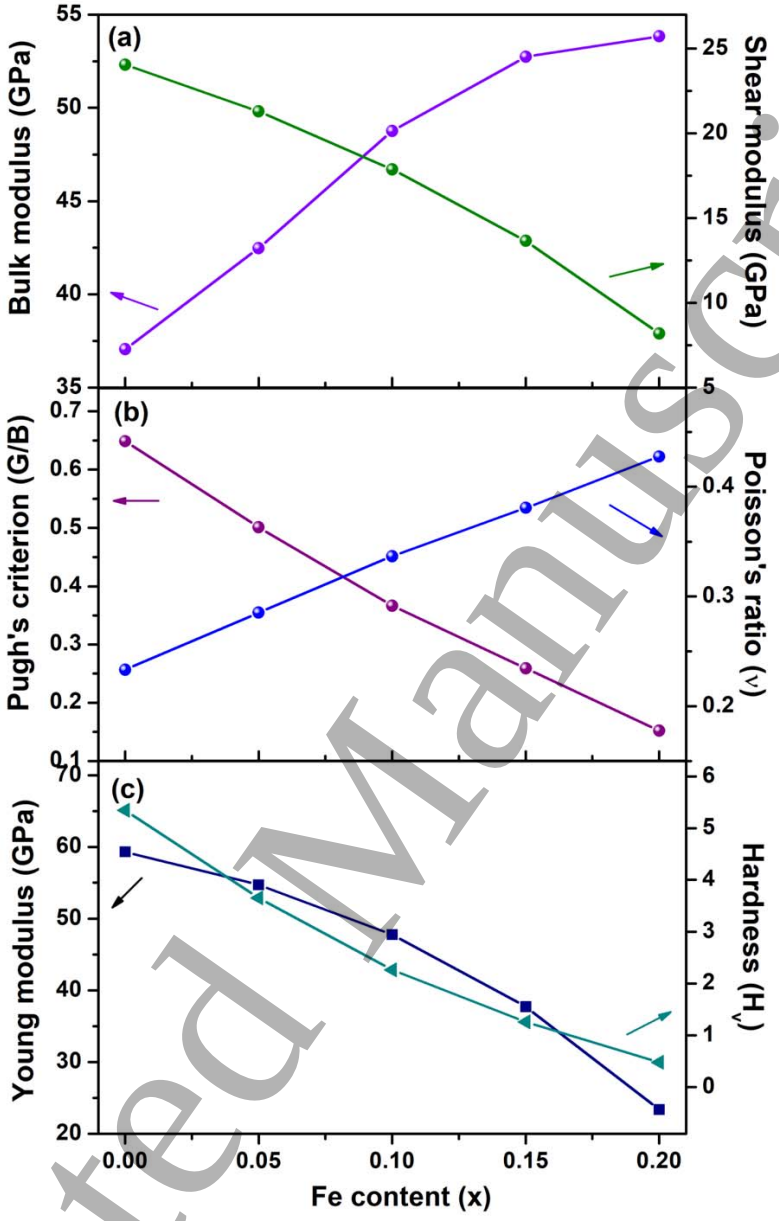

Figure 3. (a) Bulk (*B*) and shear (*G*) moduli, (b) Pugh's criterion (*G/B*) and Poisson's ratio (ν), and (c) Young's modulus (*E*) and Vickers hardness (H_v) as a function of iron content in $(Bi_{1-x}Fe_x)_2Te_3$.

Figure 3(c) shows Young's modulus and Vickers hardness (H_v) for $(Bi_{1-x}Fe_x)_2Te_3$ compounds. Young's modulus indicates the relation between stress and strain, while Vickers

hardness (H_v) is the resistance of a material to being indented. We observe that as iron is introduced into the bismuth sites these values decrease, Young's modulus indicates a decrease of ~ 60% and H_v also a reduction of 91% from Bi_2Te_3 in comparison with $(Bi_{1-x}Fe_x)_2Te_3$ when x = 0.20, indicating that the material has a lower resistance to being deformed. This behavior is in good agreement with the observed in the cell parameters, as the iron in the material increases, the change in the structure is greater. Therefore, when x = 0.20 the material reveals the greatest deformation with the increase in Fe content, the *B* modulus increases and the *G* and Young moduli decrease, which is reflected in the decrease in H_v. In Table 4 the average sound velocity (ν_m) and Debye temperature (θ_D) are shown. ν_m was calculated from the elastic constants to obtain the Debye temperature (θ_D) which is an important parameter coupled to some physical properties of materials, such as the melting temperature and specific heat. ν_m was calculated as [87] [88]: $\nu_m = \left[\frac{1}{3}\left(\frac{2}{\nu_t^3} + \frac{1}{\nu_l^3}\right)\right]^{-1/3}$ where ν_t and ν_l are the transverse and longitudinal elastic wave velocities, respectively. θ_D was calculated from ν_m as [87] [89]: $\theta_D = \frac{\hbar}{k}\left[\frac{3n}{4\pi}\left(\frac{N_A\rho}{M}\right)\right]^{1/3}\nu_m$, where $\hbar$ and k are Planck and Boltzmann´s constants respectively, n is the number of atoms per formula unit, N_A is Avogadro´s number, ρ is the density and M is the molecular mass per formula unit. From Table 4 we observe a decrease in θ_D values as iron increases in the compound, indicating that the melting temperature decreases. For x = 0.00, the computed Debye temperature value is in good agreement with the experimental one [79], showing a small error of approximately 2.4 %. Both ν_m and θ_D decrease as a function of iron content. For x = 0.2, the concentration of Bi and Te states in the conduction band near the Fermi level decrease, and together with the increase in the *3p* states of Fe they move to lower energies. This behavior causes the

hybridization between Bi and Te to decrease, reflecting an increase in the Bi/Fe-Te2 bond distance and the decrease in the *G* and *E* moduli. On the other hand, the energy gap disappears, becoming an electronic conductor and this causes, in the mechanical properties, a change to a ductile material with metallic bonds. The change in the material's ductility due to an increase in Fe has been observed in other reports [90] [91]. Furthermore, the decrease in the interaction between Te and Bi orbitals together with the interaction of Fe orbitals influence the decrease in H_v and θ_D, as these properties are linked to the interactions between the atoms of the system.

In Table 4, the mechanical properties of Bi_2Te_3-based materials, including experimental data, are displayed. In recent years, there have been published works proposing strategies to enhance the mechanical properties and machinability of Bi_2Te_3 [92] [93] while boosting the applicability in flexible devices. Samat *et al.* obtained films of a hybrid material by incorporating single-walled carbon nanotubes (SWCNTs) and Pt with nominal composition Bi_2Te_3-Pt-SWCNTs prepared by potentiostatic electrochemical deposition. Another strategy, as shown in Table 4, involves preparing commercial Bi_2Te_3 by dispersing a second phase of SiC particles in the matrix through a combined process of mechanical alloying and spark plasma sintering. In both works, the authors found improvements in mechanical properties compared to pristine Bi_2Te_3 and can be observed through variations in Young's modulus and hardness that suggest these enhancements are desirable for thermoelectric materials in flexible device applications. Therefore, Bi_2Te_3 could be used in commercial devices if the mechanical properties are improved to facilitate processing, as its chemical nature makes it easy to cause brittle fractures. The advantage of the predicted mechanical properties of $(Bi_{1-x}Fe_x)_2Te_3$ compounds supports the proposition that the incorporation of Fe can improve

mechanical properties to levels suitable for its use in commercial devices. Our results about hardness and Young's modulus are comparable to systems designed to favor machinability, as reported [92] [93]. Fe promotes the transition from brittle to metallic behavior and additionally offers the advantage of lower costs and simpler acquisition requirements compared with Bi_2Te_3-Pt-SWCNTs and Bi_2Te_3-SiC which have highly technical production methods. This newfound mechanical flexibility is crucial, especially in applications where materials need to tolerate diverse stress and adapt to dynamic conditions. The observed modifications in mechanical properties show the material's adaptability, providing a diverse range of options for technological applications. This adaptability not only deepens our understanding about the material, but also expands its potential uses across different areas, opening opportunities to take advantage of the distinctive mechanical properties introduced by iron doping.

Table 4. Bulk (B) and shear (G) moduli, Pugh's criterion (G/B), Poisson's ratio (ν), Young modulus (E), Vickers hardness (H_v), average sound velocity (v_m) and Debye temperature (θ_D) for $(Bi_{1-x}Fe_x)_2Te_3$ compounds.

Fe content (x)	B (GPa)	G (GPa)	G/B	ν	E (GPa)	H_v (GPa)	v_m (m/s)	θ_D (K)
0.00	**37.06**	**24.04**	**0.65**	**0.233**	**59.31**	**5.35**	**1830**	**168.9**
0.05	**42.48**	**21.29**	**0.50**	**0.285**	**54.72**	**3.66**	**1678**	**154.8**
0.10	**48.76**	**17.86**	**0.37**	**0.337**	**47.76**	**2.26**	**1562**	**144.4**
0.15	**52.74**	**13.66**	**0.26**	**0.381**	**37.72**	**1.26**	**1391**	**128.7**
0.20	**53.84**	**8.19**	**0.15**	**0.428**	**23.39**	**0.48**	**1150**	**106.4**
Ref. [79] **Exp.**								**164.9**
Ref. [13] **Teo.**	**36.4**	**30.2**	**0.83**	**0.180**	**71.0**			
Ref. [78] **Teo.**	**37.9**	**20.8**	**0.55**					
Ref. [14] **Teo.**	**39.7**	**24.8**	**0.83**	**0.241**			**1969**	**181.3**
Ref. [80] **Teo.**			**0.62**	**0.230**				

Ref. [69] **Teo.**	**36.4**	**30.2**	**0.83**	**0.180**		

Refs. for x = 0.00	**Bi_2Te_3 based materials experimental data**		
(*x*) content			
Pt-SWCNTs			
0.00 Ref. [92]		**20.00**	**0.40**
0.04 Ref. [92]		**100.0**	**0.60**
SiC			
0.00 Ref. [93]		**32.89**	**1.20**
0.01 Ref. [93]		**47.65**	**1.70**

3.3 Electronic properties

For Bi_2Te_3, the spin-orbit coupling (SOC) [94] is included in the calculations because Bi and Te atoms are heavy elements, its effects were treated using norm-conserving pseudopotentials. The convergence criteria for the structure optimization and energy calculations were set to ultra-fine quality with the k-point mesh of size 6×6×6, and a plane-wave cutoff energy of 300 eV.

Figure 4 shows the electronic band structure, along with the high symmetry k points in the first Brillouin zone for Bi_2Te_3 with and without SOC. The differences in energy between the bottom of the conduction band and the top of the valence band are at Γ point, indicating that Bi_2Te_3 is a direct band gap semiconductor compound with a value of 0.226 eV without SOC, and with SOC the band gap obtained was 0.138 eV, relatively close to the experimentally and theoretical results published [95] [96] [97] [98]. From Figure 4, we can observe that SOC significantly changes and affects the band structure of Bi_2Te_3. The value of the energy gap between the approximation with and without SOC has a very significant difference of around 64%, however, both values are in accordance with the experimental values, as shown in Table 5.

Table 5. Bi_2Te_3 band gap results compared with previous first-principles calculations and experimental data.

Methodology	Reference	Band gap (eV)	Type of band gap
GGA-PBEsol	**This work**	**0.226**	**Direct**
GGA-PBEsol-SOC	**This work**	**0.138**	**Direct**
Experimental	[29]	**0.241**	
Experimental	[95]	**0.160**	**Indirect**
Experimental at 10K	[98]	**0.150**	**Indirect**
Experimental at 10K	[98]	**0.220**	**Direct**
LAPW	[98]	**0.170**	**Direct**
GGA-PBE	[80]	**0.256**	**Direct**
GGA-PBE	[67]	**0.271**	**Direct**
GGA-PBE+SOC	[67]	**0.105**	**Direct**
LDA	[97]	**0.230**	**Direct**
LDA+SOC	[97]	**0.150**	**Indirect**
LDA	[99]	**0.110**	**Indirect**
GGA-PBE	[100]	**0.910**	**Indirect**
LAPW	[95]	**0.370**	**Direct**
LAPW+SOC	[95]	**0.130**	**Indirect**

Regarding the band structure of Bi_2Te_3 with SOC, we observe a direct band gap around the Γ point for x = 0.00 with E_g = 0.138 eV, this indicates a semiconductor behavior. This value is very close to the one experimentally observed by Thomas *et al*. at 10 K with E_g = 0.15 eV, in good agreement with other reports [24] [45] [98]. Lou *et al*. reported E_g = 0.241 eV [29] and the theoretical calculated by J. Fu *et al*. of 0.256 eV [80], these values are close to the value obtained in this work without SOC.

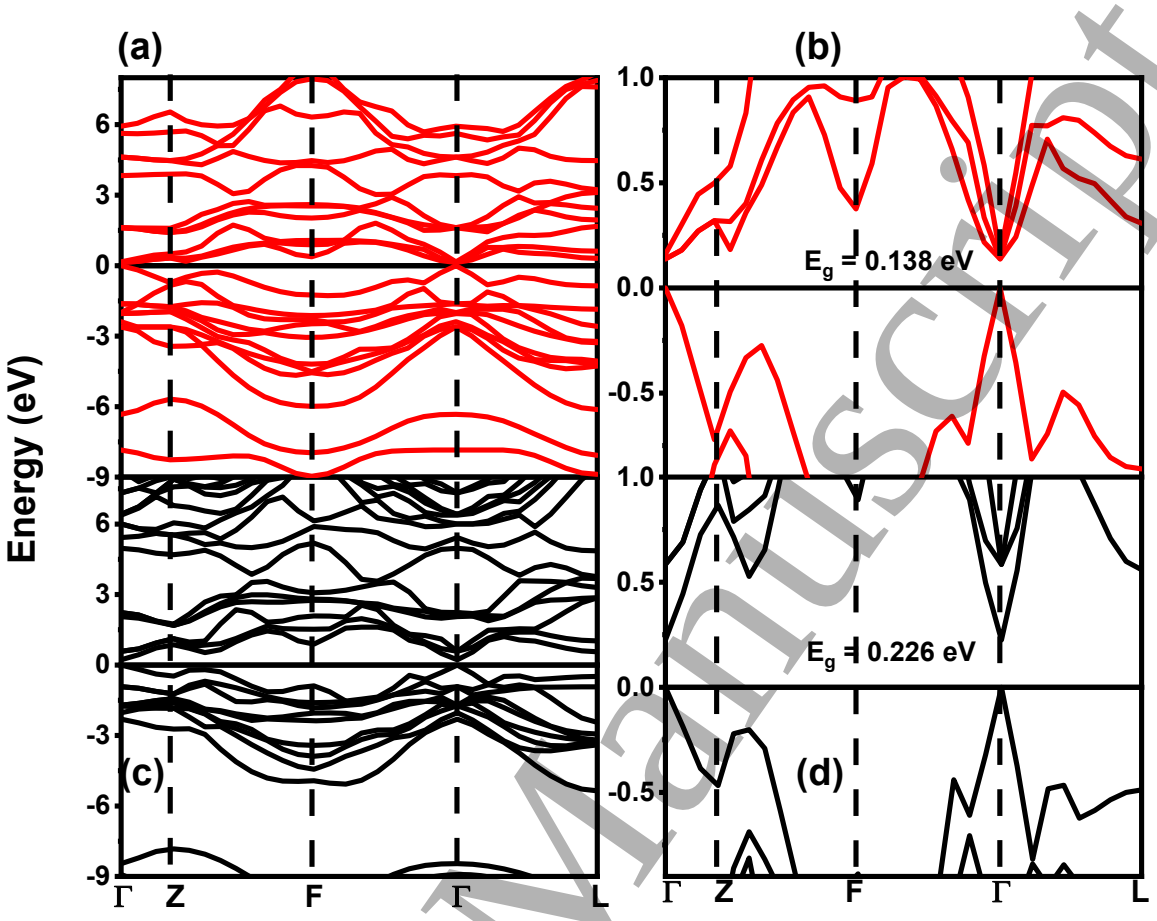

Figure 4. Band structure of Bi_2Te_3 (a) with SOC and (c) without SOC at energy range − 9 eV to 8 eV, and zoom (b) with SOC and (d) without SOC at energy range −0.9 eV to 1.0 eV.

The total density of states near the Fermi level for $(Bi_{1-x}Fe_x)_2Te_3$ is shown in Figure 5. At the Fermi level, for x = 0.00, the semiconductor behavior is observed, as Fe is introduced a conductor behavior is confirmed. Near the Fermi level the contribution of the DOS increases as Fe is introduced, the inset in Figure 5 shows the DOS value at $N(E_F = 0)$ as a function of Fe content. Therefore, a modulation of the DOS at $N(E_F = 0)$ could be done depending on iron content as previously reported by XPS valence band spectra [48]. Due to the decrease in Bi atoms, the contributions of Bi *6p* orbitals and Te *5p* orbitals shift to lower energy levels.

On the other hand, near the Fermi level (from -5 to 0 eV) the increase in Fe atoms causes Te *5s* orbitals to interact with Bi *6p*, Fe *3p* and Fe *4s* orbitals, Figure 6; therefore, small amounts of iron modify the DOS near the Fermi level, causing a decrease in intensity. Although, at $N(E_F = 0)$ a linear increase of electronic states is observed as a function of Fe content in the compound.

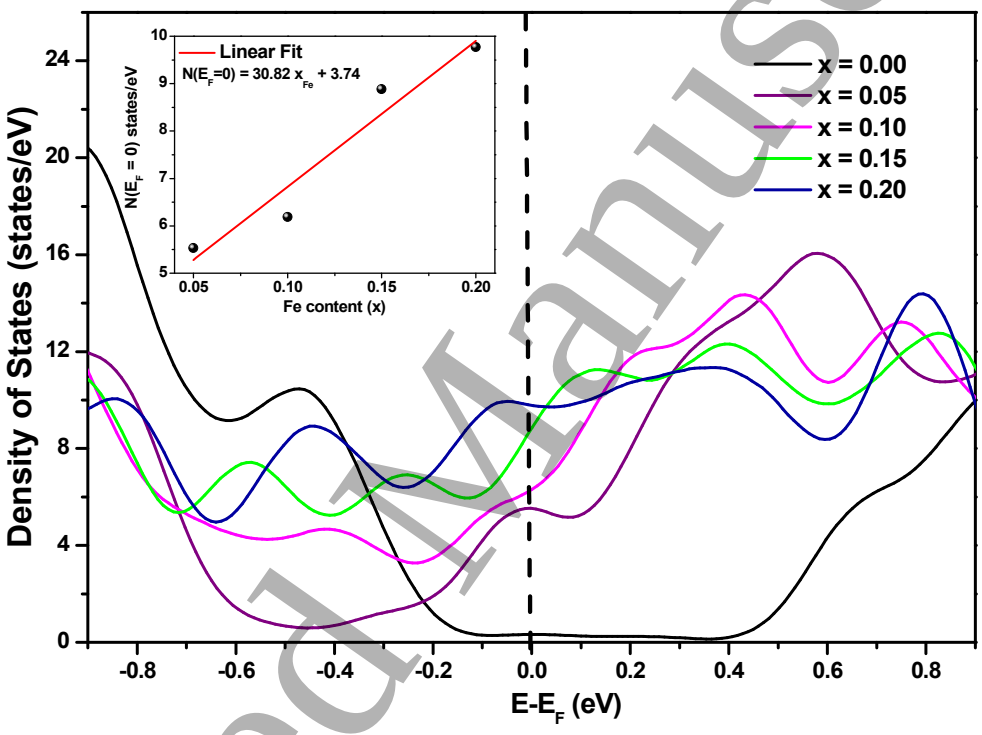

Figure 5. The density of states of $(Bi_{1-x}Fe_x)_2Te_3$ near the Fermi level, the inset shows the behavior of the DOS at the Fermi level as a function of iron content.

Finally, the total and partial density of states (PDOS) for $(Bi_{1-x}Fe_x)_2Te_3$ is shown in Figure 6. Near the Fermi level, for x = 0.00, Figure 6(a), shows that the contributions to the occupied states come from Te 5p orbitals, while in the unoccupied states contributions are provided by Bi 6*p* orbitals. As iron is introduced into the compound, Te *5p* orbitals and Bi/Fe *p* orbitals remain in the occupied and unoccupied states, respectively, Figure 6(b-d). Also, when x =

0.20, the major contribution to the DOS from -5 to 3 eV comes from Te *5p* orbitals; this implies that in both the occupied and unoccupied states the contribution is dominated by this orbital, Figure 6(e). In the lowest energy region from -15 to -8 eV, the contribution to the density of states is dominated by the Bi/Fe *s* orbitals and Te *5s* orbitals for the studied compounds. Furthermore, the displacement towards lower energies respecting DOS, also generates a rise in the contribution to the PDOS at the Fermi level for Bi/Fe *p* orbitals and Te *5p* orbitals. The behavior observed in the PDOS suggests a strong hybridization between Te *5p* orbitals and Bi *6p* orbitals from -5 to 0 eV for Bi_2Te_3, which agrees with other theoretical calculations [101] [102]. Moreover, the greatest contribution around the Fermi level comes from *s* and *p* orbitals, both from Bi/Fe and Te. As shown, Bi *p* orbitals (x = 0.0) are at ~1.2 eV; when Fe is introduced into the compound, these shift towards lower energies, which causes the DOS at the Fermi level to gradually increase with the increase in Fe content. This could be explained as follows: in Bi_2Te_3 a strong bond between Bi *6p* orbitals and Te *5s* and Te *5p* orbitals exists, in accordance with the Bi-Te2 bond length shown in Table 1. When substituting Fe in Bi sites, the bond between Bi *6p* orbitals and Te *5s* and Te *5p* begins to delocalize, decreasing the states and shifting to lower energies, this causes an increase in the Bi/Fe-Te2 bond distance and a decrease in the bond angles Bi/Fe-Te1-Bi/Fe and Te2-Bi/Fe-Te1, Table 1. The delocalized electrons are due to the electronegativity values, iron has 1.83, less than 2.02 for Bi, so the introduction of Fe into the system makes the valence electrons more free and therefore less energy is required to pass from the valence band to the conduction one. This combined with the small energy gap of 0.226 eV that the compound has when it is not doped (Bi_2Te_3), allows the incorporation of Fe to cause conductive behavior which increases as the Fe content increases, as shown in Figure 6.

According to the DOS, Bi_2Te_3 is a semiconductor material with an energy bad gap of 0.226 eV. By introducing small amounts of Fe as dopant, a change from semiconductor to conductor behavior is observed. Increasing the amount of dopant, we observe and increase of the DOS at the Fermi level, which indicates that a gradual modulation of the DOS at the Fermi level occurs. Therefore, if the Fermi level is modulated due to small magnetic impurities electronic states such as the Quantum Anomalous Hall Effect and the topological magnetoelectric effect can be widely studied to improve the performance of electronic components, which could generate a new branch of computing based on quantum topology with high fault tolerance [103].

Moreover, Bi_2Te_3 is a material widely used in thermoelectric (TE) generators, nevertheless its use is limited because they are rigid and fragile [104]. The change to an electronic conductor and flexible material by adding Fe to Bi_2Te_3, may favor its use as a flexible polyimide film in flexible thermoelectric generators that can be used in micropower systems applied in self-powered sensors and electronic devices [104] [105]. Applied as a material in thermoelectric devices (TEDs), the increase in the flexibility of Bi_2Te_3 with Fe can reduce the excessive use of welding with the electrodes to avoid serious defects in the system due to thermal expansion [106] which would lead to the use of this material for applications in power supplies and localized cooling [107], medicine [108], transistors [109], chip and solar thermoelectric applications [110].

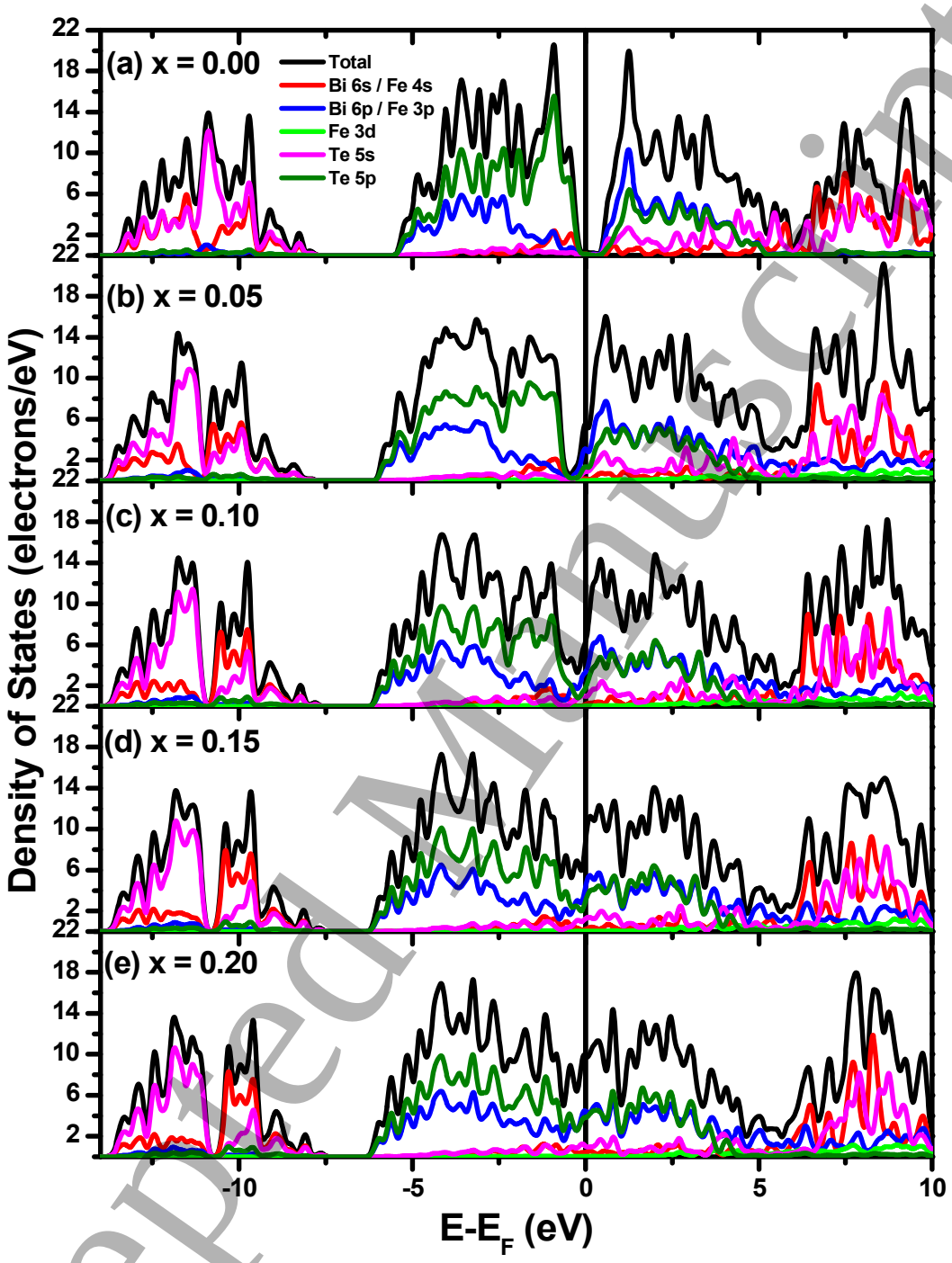

Figure 6. Partial density of states as a function of iron content (x) in $(Bi_{1-x}Fe_x)_2Te_3$, (a) x = 0.00, (b) x = 0.05, (c) x = 0.10, (d) x = 0.15, and (e) x = 0.20.

Due to the limited reports in the literature on the studied system, Table 6 shows data regarding mechanical, thermoelectric, and electronic properties. The aim is to compare the results obtained in this work with those reported in some related materials. Concerning B, it can be observed that the values from reference [4] are the closest to our results for the system without Fe substitution. In the case of E, G, ν, and G/B, the values reported in [4] are in good agreement with our results. Regarding the thermoelectric figure of merit, ZT, it is interesting to note that the reported values do not follow a clear trend. However, the highest value obtained is 1.04 for the Bi_2Te_3 + 0.1 vol% SiC system. Additionally, the band gap values corroborate the semiconductor character reported in various theoretical and experimental works. Finally, for $(Bi_{0.8}Fe_{0.2})_2Te_3$ significant modifications of the properties studied here are observed, clearly demonstrating that the substitution of Bi by Fe significantly contributes to the modification of the physical properties discussed in previous sections.

Table 6. Mechanical, thermoelectric and electronic properties of Bi2Te3 based materials.

Material	*B* (GPa)	*G* (GPa)	*E* (GPa)	*ν*	H_ν (GPa)	*G/B*	*ZT*	Band gap (eV)
Bi_2Te_3 this work	**37.06**	**24.04**	**59.31**	**0.23**	**5.35**	**0.65**		**0.14 (SOC)**
$(Bi_{0.8}Fe_{0.2})_2Te_3$ this work	**53.84**	**8.19**	**23.39**	**0.43**	**0.48**	**0.15**		
Bi_2Te_3 [111] [a]	**40.31**							
Bi_2Te_3 [112] [b]	**37.4**		**54.2 (in plane)**					
Bi_2Te_3 [113] [c]	**31.6**		**51.4 (in plane)**				**~0.55 (300K)**	**0.13**
Bi_2Te_3 [114] [d] **(un-annealed)**							**0.06 (300 K)**	**0.16**
Bi_2Te_3 [114] [d] **(annealed)**							**0.19 (300 K)**	**0.11**
$Bi_{0.5}Sb_{1.5}Te_3$ (ZM) [4] [e]	**38.0**	**24.0**	**59.0**	**0.24**	**~0.25**	**0.63**		

$Bi_{0.5}Sb_{1.5}Te_3$ (MS-PAS) [4] [e]	**29.0**	**20.0**	**50.0**	**0.22**	**~0.40**	**0.69**	
$Bi_{0.4}Sb_{1.6}Te_3$ + 0.5 wt% CNTs [115] **(BM-SPS)** [f]		**18.0**	**45.0**	**0.25**			
Bi_2Te_3 + 0.1 vol% SiC [d] [116] **(BM-SPS)**			**~37**		**~0.70**		**1.04 (423 K)**
$Mg_{0.01}Bi_{1.99}Te_3$ [117] [d]							**0.8 (350 K)**

[a] Theoretical GGA-PBE, [b] Ultrasonic experiment at 280 K, [c] Theoretical LDA CA-PZ, [d] Experimental, [e] ZM = zone melted, MS-PAS = melt spinning combined with a plasma-activated sintering, [f] BM-SPS = ball milling spark plasma sintering.

4. Conclusions

In this work, the crystal structure, and elastic and electronic properties of $(Bi_{1-x}Fe_x)_2Te_3$ were studied by first-principles calculations within the generalized gradient approximation with PBEsol functional. The crystal structure results agree with experimental and theoretical reported data. We found that the unit cell volume decreases as Fe is introduced in bismuth sites. The elastic constants indicate that the system is mechanically stable. According to Pugh's criterion and Poisson's ratio, the system changes from a brittle material with ionic-covalent bonds to a ductile material with metallic bonds as iron content increases and Vickers hardness in the compound decreases. Poisson's ratio changes as iron substitutes bismuth, indicating that there is an ionic-covalent bond for x = 0.00 and behave like metal as iron content increase. The band structure shows a direct band gap at Γ point for Bi_2Te_3, indicative of a semiconductor behavior; nevertheless, as iron is introduced, the band gap vanishes, indicating a conductor behavior. Furthermore, the total density of states at the Fermi level increases as iron content increases. The contribution to the occupied states at the Fermi level is provided by Te *5p* orbitals, while the unoccupied states come from Bi *6p* orbitals for

Bi_2Te_3, as Fe is introduced in bismuth sites, this behavior is maintained. Finally, the PDOS shows a slight displacement towards lower energies promoted by the increase of iron and decrease of Bi content in the compound; this also generates a rise in the contribution to the DOS at the Fermi level. Besides, the increased iron in the structure generates an interaction between Fe *3p* orbitals and Te *5s* orbitals. The transition from intrinsic brittleness to enhanced flexibility, coupled with a shift to a conductive regime, holds promising implications, particularly in the domain of flexible thermoelectric devices where the traditionally rigid and fragile nature of Bi_2Te_3 becomes a limiting factor. The introduction of iron emerges as a decisive factor, potentially unlocking new paths in the development of flexible electronic devices and enabling a transition from conventional semiconductor behavior to a ductile conductor.

Acknowledgments

The authors acknowledge the financial support from projects DGAPA-UNAM IA103923, IN100222, and IN103923. Programa de Apoyo a Proyectos para Innovar y Mejorar la Educación (PAPIME) with project number PE101723. We thank the Supercomputing Center DGTIC-UNAM and Laboratorio Nacional de Supercómputo del Sureste de México for the resources provided for performing the calculations in this work. J.L. Rosas-Huerta acknowledges the postdoctoral-scholarship granted by Secretaría de Educación, Ciencia, Tecnología e Innovación de la Ciudad de México (SECTEI/098/2022). J. Pilo and J. E. Antonio acknowledge the postdoctoral grant by Dirección General de Asuntos del Personal Académico: Programa de Becas Posdoctorales, UNAM. H. Muñoz acknowledges the financial support from CONAHCYT and BEIFI-IPN. Also, the authors want to thank F. Sarmiento and A. Tejeda-Cruz for their technical support.

AUTHOR CONTRIBUTION STATEMENT

E. P. Arévalo-López conceived the original idea and wrote the manuscript. J. L. Rosas-Huerta, J. Pilo, J. E. Antonio, H. Muñoz and A. Benitez-Rico contributed and discussed the obtained data. R. Escamilla, and M. Romero contributed and discussed the final version of the manuscript.

References

[1] H. Zhang, C.-X. Liu, X.-L. Qi, X. Dai, Z. Fang, and S.-C. Zhang, Nat. Phys. 5, 438 (2009)..

[2] S. V. Eremeev, Yu. M. Koroteev, and E. V. Chulkov, JETP. Lett. 91, 387 (2010)..

[3] S. V. Eremeev, G. Landolt, T. V. Menshchikova, et al. Nat. Commun. 3, 635 (2012).

[4] Y. Zheng, X. Y. Tan, X. Wan, X. Cheng, Z. Liu, and Q. Yan ACS Appl. Energy Mater. 2020, 3, 3, 2078–2089 https://doi.org/10.1021/acsaem.9b02093.

[5] Heremans, J., Cava, R. & Samarth, N. Nat Rev Mater 2, 17049 (2017). https://doi.org/10.1038/natrevmats.2017.49.

[6] Cava, R. J., Ji, H., Fuccillo, M. K., Gibson, Q. D. & Hor, Y. S. J. Mat. Chem. C 1, 3176–3189 (2013).

[7] Ando, Y. J. Phys. Soc. Jpn 82, 102001 (2013).

[8] He, J.; Tritt, T. M. Science 2017, 357, 1369..

[9] Zhu, T.; Hu, L.; Zhao, X.; He, J. Adv. Sci. 2016, 3, 1600004..

[10] Mamur, H.; Bhuiyan, M. R. A.; Korkmaz, F.; Nil, M.. Renewable Sustainable Energy Rev. 2018, 82, 4159−4169.

[11] Shi, X.; Chen, L.; Uher, C. Int. Mater. Rev. 2016, 61, 379.

[12] Su, X.; Wei, P.; Li, H.; Liu, W.; Yan, Y.; Li, P.; Su, C.; Xie, C.; Zhao, W.; Zhai, P.; Zhang, Q.; Tang, X.; Uher, C. Adv. Mater. 2017, 29, 1602013.

[13] [Z. Xiong, X. An, Z. Li, T. Xiao, X. Chen, Journal of Alloys and Compounds, Volume 586, 2014, Pages 392-398, https://doi.org/10.1016/j.jallcom.2013.10.062.

[14] H. Koc, A. M. Mamedov and E. Ozbay, Joint UFFC, EFTF and FM Symposium, 41–44 (2013).

[15] J.Fu, J. Huang, F. Bernard Composites Communications Volume 28, December 2021, 100917 https://doi.org/10.1016/j.coco.2021.100917.

[16] Z. Xiong et al. Journal of Alloys and Compounds 586 (2014) 392-398..

[17] Y.-K. Zhu, P. Wu, J. Guo, Y. Zhou, X. Chong, Z.-H. Ge, J. Feng Ceramics International 46 (2020) 14994-15002 https://doi.org/10.1016/j.ceramint.2020.03.029.

[18] Li, JF., Liu, WS., Zhao, LD. et al. NPG Asia Mater 2, 152–158 (2010). https://doi.org/10.1038/asiamat.2010.138.

[19] A. I. Figueroa, G. van der Laan, L. J. Collins-McIntyre, S.-L. Zhang, A. A. Baker, S. E. Harrison, P. Schönherr, G. Cibin, and T. Hesjedal Phys. Rev. B 90, 134402 https://doi.org/10.1103/PhysRevB.90.134402.

[20] L. B. Duffy, A. I. Figueroa, Ł. Gładczuk, N.-J. Steinke, K. Kummer, G. van der Laan, and T. Hesjedal Phys. Rev. B 95, 224422 DOI: 10.1103/PhysRevB.95.224422.

[21] M. F. Islam, C. M. Canali, A. Pertsova, et al. Phys. Rev. B 97, 155429 https://doi.org/10.1103/PhysRevB.97.155429.

[22] Figueroa, A., van der Laan, G., Harrison, S. et al. Sci Rep 6, 22935 (2016). https://doi.org/10.1038/srep22935.

[23] Yurong Ruan et al 2019 J. Phys.: Condens. Matter 31 385501 DOI 10.1088/1361-648X/ab2705.

[24] Y. S. Hor, A. J. Williams, J. G. Checkelsky et al. Phys. Rev. Lett. 104, 057001 (2010) https://doi.org/10.1103/PhysRevLett.104.057001.

[25] P. Arévalo-López, F. Morales-Leal, and R. Escudero-Derat, J. Mex. Chem. Soc 60, 101–107 (2016) https://www.scielo.org.mx/pdf/jmcs/v60n3/1870-249X-jmcs-60-03-00101.pdf.

[26] A.I. Figueroa, G. van der Laan, L.J. Collins-McIntyre, G. Cibin, A.J. Dent, T. Hesjedal, J. Phys. Chem. C 119 (2015) 17344–17351, https://doi.org/10.1021/jp511713s.

[27] D. West, Y.Y. Sun, S.B. Zhang, X. Ma, X. Chen, J.F. Jia, Q.-K. Xue, Phys. Rev. B 85 (2012) 081305(R), https://doi.org/ 10.1103/PhysRevB.85.081305.

[28] K. Momma and F. Izumi, J. Appl. Crystallogr. 44, 1272–1276 (2011) https://doi.org/10.1107/S0021889811038970..

[29] L.-Y. Lou, J. Yang, Y.-K. Zhu, H. Liang, Y.-X. Zhang, J. Feng, J. He, Z.-H. Ge, L.-D. Zhao Advanced Science 2022, 9 (27) https://doi.org/10.1002/advs.202203250.

[30] J.-B. Vaney S. Aminorroaya Yamini, H. Takaki, K. Kobayashi, N. Kobayashi, T. Mori Materials Today Physics 9 (2019) 1000902 https://doi.org/10.1016/j.mtphys.2019.03.004.

[31] Andrzej Ptok et al 2021 J. Phys.: Condens. Matter 33 065501 DOI 10.1088/1361-648X/abba6a.

[32] X Y Wei Physics Letters A 379, 5, 2015, Pages 417-420 https://doi.org/10.1016/j.physleta.2014.11.032.

[33] W. Niu, K. Du, S. Wang et al. Nanoscale, 2017,9, 12372-12378 https://doi.org/10.1039/C7NR02807E.

[34] N. H. Jo, K. J. Lee, C. M. Kim, et al. Phys. Rev. B 87, 201105(R) https://doi.org/10.1103/PhysRevB.87.201105.

[35] Y. Takagaki, J. Herfort, M. Ramsteiner, U. Jahn, B. Jenichen CrystEngComm, 2018, 20, 4173-4178 https://doi.org/10.1039/C8CE00882E.

[36] V. M Pereira, C. N. Wu, C.-A. Knight, A. Choa, L. H. Tjeng, S. G. Altendorf APL Mater. 8, 071114 (2020) https://doi.org/10.1063/5.0010339.

[37] Tokura, Y., Yasuda, K., Tsukazaki, A. Nat Rev Phys 1, 126–143 (2019). https://doi.org/10.1038/s42254-018-0011-5.

[38] K. Nomura, N. Nagaosa 2011 Phys. Rev. Lett. 106 166802 https://doi.org/10.1103/PhysRevLett.106.166802.

[39] R. Yu, W. Zhang, H. J. Zhang, S. C. Zhang, X. Dai, Z. Fang 2010 Science 329 5987 doi: 10.1126/science.1187485.

[40] N. S. Kander, S. Guchhait, A. K. Das 2023 Phys. Scr. 98 035802 https://doi.org/10.1088/1402-4896/acb513.

[41] W. K. Tse, A. H. Macdonald 2010 Phys. Rev. Lett. 105 057401 https://doi.org/10.1103/PhysRevLett.105.057401.

[42] P. Wang, J. Ge, J. Li, Y. Liu, Y. Xu, J. Wang The Innovation 2, 2, 100098 2021 https://doi.org/10.1016/j.xinn.2021.100098.

[43] H. Yang, L. G. Liu, M. Zhang, X. S. Yang Solid State Communications 241 (2016) 26–31 https://doi.org/10.1016/j.ssc.2016.05.008.

[44] J. Ge, T. Chen, M. Gao, X. Wang, et al. Solid State Comm 211 (2015) 29-33, http://dx.doi.org/10.1016/j.ssc.2015.03.012.

[45] S. Cichoň, V. Drchal, K. Horáková, V. Cháb, I. Kratochvílová, F. Máca, P. Čermák, K. Čermák, J. Navrátil, J. Lančok The Journal of Physical Chemistry C 2022 126 (34), 14529-14536 DOI: 10.1021/acs.jpcc.2c02724.

[46] S. Byun, J. Cha, C. Zhou, Y. K. Lee, H. Lee, S. H. Park, W. B. Lee, I. Chung Journal of Solid State Chemistry 269 (2019) 396-400 https://doi.org/10.1016/j.jssc.2018.10.012.

[47] N. S. Kander, S. Islam, S. Guchhait, A. K. Das App Phys A 2023 129, 253 https://doi.org/10.1007/s00339-023-06524-1.

[48] E.P. Arévalo-López, P. Romero-Moreno, J.L. Rosas-Huerta, L. Huerta, Claire Minaud, M.L. Marquina, R. Escamilla, M. Romero Journal of Alloys and Compounds 899 (2022) 163297 https://doi.org/10.1016/j.jallcom.2021.163297.

[49] [S.J. Clark, M.D. Segall, C.J. Pickard, P.J. Hasnip, M.I.J. Probert, K. Refson, M.C. Payne, Z. Krist. 220 (2005) 567–570, https://doi.org/10.1524/zkri.220.5.567.65075.

[50] M.D. Segall, P.J.D. Lindan, M.J. Probert, C.J. Pickard, P.J. Hasnip, S.J. Clark, M.C. Payne, J. Phys. Condens. Matter 14 (2002) 2717–2744, https://doi.org/10.1088/0953-8984/14/11/301.

[51] W. Kohn, L.J. Sham, Phys. Rev. 140 (1965) A1133–A1138, https://doi.org/10.1103/PhysRev.140.A1133.

[52] P. E. Blöchl, Phys. Rev. B 50, 17953 (1994) https://doi.org/10.1103/PhysRevB.50.17953.

[53] G. Kresse and D. Joubert, Phys. Rev. B 59, 1758 (1999) https://doi.org/10.1103/PhysRevB.59.1758.

[54] J. P. Perdew, K. Burke, and M. Ernzerhof, Phys. Rev. Lett. 77, 3865 (1996) https://doi.org/10.1103/PhysRevLett.77.3865.

[55] J. P. Perdew, A. Ruzsinszky, G. I. Csonka, O. A. Vydrov, G. E. Scuseria, L. A. Constantin, X. Zhou, and K. Burke, Phys. Rev. Lett. 100, 136406 (2008) https://doi.org/10.1103/PhysRevLett.100.136406.

[56] S. Nakajima, J. Phys. Chem. Solids 24, 479 (1963).

[57] S. Wang, C. Zhang, X. Li, H. Huang, J. Wang, J. Mater. Sci. Technol. 58 (2020) 205–214, https://doi.org/10.1016/j.jmst.2020.03.065..

[58] S. Wang, Y. Zhao, S. Deng, W. Yang, D. Lian, H. Hou, J. Phys. Chem. Solid. 125 (2019) 115–122, https://doi.org/10.1016/j.jpcs.2018.10.020..

[59] H.J. Monkhorst, J.D. Pack, Phys. Rev. B 13 (1976) 5188–5192, https://doi.org/10.1103/PhysRevB.13.5188.

[60] Bellaiche, L. and Vanderbilt, D., Phys. Rev. B 61 (12), 7877—7882, 2000 http://doi.org/10.1103/PhysRevB.61.7877.

[61] B.G. Pfrommer, M. Côté, S.G. Louie, M.L. Cohen, J. Comput. Phys. 131 (1997) 233–240, https://doi.org//10.1006/jcph.1996.5612..

[62] D. Vanderbilt, Phys. Rev. B 41, 7892–7895 (R) (1990).https://doi.org/10.1103/PhysRevB.41.7892..

[63] R. D. Shannon Acta Cryst. (1976). A32, 751-767 https://doi.org/10.1107/S0567739476001551.

[64] J. Choi, H.-W. Lee, B.-S. Kim, S. Choi, J. Choi, J.H. Song, S. Cho, J. Appl. Phys. 97 (2005) 10D324, https://doi.org/10.1063/1.1854451.

[65] Z. Wang, A.A. Taskin, T. Frölich, M. Braden, Y. Ando, S Chem. Mater. 28 (2016) 779–784, https://doi.org/10.1021/acs.chemmater.5b03727.

[66] Y.S. Hor, P. Roushan, H. Beidenkopf, J. Seo, D. Qu, J.G. Checkelsky, L.A. Wray, D. Hsieh, Y. Xia, S.-Y. Xu, D. Qian, M.Z. Hasan, N.P. Ong, A. Yazdani, R.J. Cava, Phys. Rev. B 81 (2010) 195203, https://doi.org/10.1103/PhysRevB.81.195203.

[67] B. Ryu, B. S. Kim, J. E. Lee, et al. Journal of the Korean Physical Society 68, 115–120 (2016). https://doi.org/10.3938/jkps.68.115.

[68] K. Zhao, Y. Wang, C. Xin, Y. Sui, X. Wang, Y. Wang, Z. Liu, B. Li Journal of Alloys and Compounds 661, 2016, 428-434 https://doi.org/10.1016/j.jallcom.2015.11.192.

[69] Z. Xiong, X. An, Z. Li, T. Xiao, X. Chen, Journal of Alloys and Compounds 586 (2014) 392-398 https://doi.org/10.1016/j.jallcom.2013.10.062.

[70] Li Ma, Jianguang Wang, Jijun Zhao, Guanghou Wang, Chemical Physics Letters, Volume 452, Issues 1–3, 2008 https://doi.org/10.1016/j.cplett.2007.12.054.

[71] M. D. Watson, L. J. Collins-MCIntyre, L. R. Shelford, et al. 2013 New J. Phys. 15 103016 DOI 10.1088/1367-2630/15/10/103016.

[72] M.M. Nassary, H.T. Shaban, M.S. El-Sadek, Materials Chemistry and Physics, 113, 1, 2009, Pages 385-388, https://doi.org/10.1016/j.matchemphys.2008.07.106.

[73] Y. Kumar, R. Sultana, V.P.S. Awana, Physica B: Condensed Matter, Volume 609, 2021, 412759, https://doi.org/10.1016/j.physb.2020.412759.

[74] Lange, P. W.(1939). Ein Vergleich zwischen Bi2Te3 und Bi2Te2S. Naturwissenschaften, 27.

[75] R. Gaillac, P. Pullumbi, F.-X. Coudert J. Phys. Condens. Matter, 2016, 28, 275201 DOI 10.1088/0953-8984/28/27/275201.

[76] N. Narendra, P. Noroizzadeh, D. Vashaee, K. W. Kim Appl. Phys. Lett. 111, 232101 (2017) https://doi.org/10.1063/1.4989602.

[77] F. Mouhat and F.-X. Coudert PHYSICAL REVIEW B 90, 224104 (2014) DOI: 10.1103/PhysRevB.90.224104.

[78] E. Güler and M. Güler, International Journal of Modern Physics B Vol. 29, No. 31 (2015) 1550222 https://doi.org/10.1142/S0217979215502227.

[79] J.O. Jenkins, J.A. Rayne and R.W. Ure Elastic moduli and phonon properties of Bi2Te3 Phys. Rev. B, 5 (1972), pp. 3171-3184.

[80] J. Fu, J. Huang, F. Bernard Composites Communications 28 (2021) 100917 https://doi.org/10.1016/j.coco.2021.100917.

[81] W. Voigt, Lehrbuch der Kristallphysik (Textbook of crystal physics), BG Teubner, Leipzig Und Berlin, 1928.

[82] A. Reuss, Calculation of the flow limits of mixed crystals on the basis of the plasticity of monocrystals, Z. Angew. Math. Mech. 9 (1929) 49–58..

[83] R. Hill, The elastic behaviour of a crystalline aggregate, Proc. Phys. Soc. 65 (1952) 349–354, https://doi.org/10.1088/0370-1298/65/5/307.

[84] J. Haines, J. M. Leger, and G. Bocquillon, Annu. Rev. Mater.Res.31, 1 (2001). https://doi.org/10.1146/annurev.matsci.31.1.1.

[85] S.F. Pugh, XCII. Relations between the elastic moduli and the plastic properties of polycrystalline pure metals, The London, Edinburgh, and Dublin Philosophical Magazine and Journal of Science 45 (1954) 823–843, https://doi.org/10.1080/14786440808520496.

[86] P. H. Mott and C. M. Roland Phys. Rev. B (2009) 80, 132104 https://doi.org/10.1103/PhysRevB.80.132104.

[87] O. Anderson, J. Phys. Chem. Solids.24, 909-917 (1963) https://doi.org/10.1016/0022-3697(63)90067-2.

[88] H. Koc, S. Simsek, S. Palaz, O. Oltulu, A. Mamedov, E. Ozbay, Physica Status Solidi (c), 2015, 12 (6) DOI: 10.1002/pssc.201400245.

[89] I. Johnston, G. Keeler, R. Rollins, and S. Spicklemire, Solids State Physics Simulations, The consortium for upperlevel physics software (Wiley, New York, 1996).

[90] Sandeep Nambiar S., BRN. Murthy, Sathyashankara Sharma, A. A. Prasanna, Arout Chelvane J Eng. Sci., 2022, 17, 303–308 https://dx.doi.org/10.30919/es8d632.

[91] S. Shu, F. Qiu, C. Tong, X. Shan, Q. Jiang Journal of Alloys and Compounds 2014, 617, 302-305, https://doi.org/10.1016/j.jallcom.2014.07.199.

[92] Samat, K.F., Li, Y., Van Toan, N. et al. Journal of Materials Research 37, 3445–3458 (2022). https://doi.org/10.1557/s43578-022-00694-z.

[93] Yu-Ke Zhu, Peng Wu, Jun Guo, Yunxuan Zhou, Xiaoyu Chong, Zhen-Hua Ge, Jing Feng, Ceramics International, Volume 46, Issue 10, Part A, 2020, Pages 14994-15002, https://doi.org/10.1016/j.ceramint.2020.03.029.

[94] WG Richards, H.-P. Trivedi, D.L. Cooper, Spin-Orbit Coupling in Molecules, Oxford University Press, 1981.

[95] P. Larson, S. Mahanti, M.G. Kanatzidis, Phys. Rev. B 61 (2000) 8162. https://doi.org/10.1103/PhysRevB.61.8162.

[96] M. Takashiri, Y. Asai, K. Yamauchi, Nanotechnology 27 (2016) 335703. 10.1088/0957-4484/27/33/335703.

[97] M.Z. Mohyedin, M.F.M. Taib, A. Radzwan, A. Shaari, M. Mustaffa, B.U. Haq, M.Z.A. Yahya, Computational and Theoretical Chemistry, 1182 (2020) 112851. https://doi.org/10.1016/j.comptc.2020.112851.

[98] G. A. Thomas, D. H. Rapkine, R. B. Van Dover, L. F. Mattheiss, W. A. Sunder, L. F. Schneemeyer, and J. V. Waszczak Phys. Rev. B 1992, 46, 1553 https://doi.org/10.1103/PhysRevB.46.1553.

[99] Yavorsky, B. Yu. and Hinsche, N. F. and Mertig, I. and Zahn, P. Phys. Rev. B 84 (2011) 165208 https://doi.org/10.1103/PhysRevB.84.165208.

[100] X. Li, H. Ren, Y. Luo, Appl. Phys. Lett. 98 (2011) 083113. https://doi.org/10.1063/1.3556654.

[101] P. Larson and W. R. L. Lambrecht, Phys. Rev. B, vol. 78, p. 195207, 2008.

[102] Y. R. Guo, C. Giao, J. J. Wang, H. Shen, S. Y. Wang, Y. X. Zheng, R. J. Zhang, L. Y. Chen, W.-S. Su, C. Z. Wang y K. M. Ho, New J. Phys., vol. 21, p. 093062, 2019.

[103] Yuanyang Deng 2022 J. Phys.: Conf. Ser. 2386 012058 doi:10.1088/1742-6596/2386/1/012058.

[104] H. You, Z. Li, Y. Shao, X. Yuan, W. Liu, H. Tang, Q. Zhang, Y. Yan, X. Tang, Applied Thermal Engineering, 202, 2022, 117818.

[105] Yang, S., Li, Y., Deng, L. et al. Flexible thermoelectric generator and energy management electronics powered by body heat. Microsyst Nanoeng 9, 106 (2023). https://doi.org/10.1038/s41378-023-00583-3.

[106] W.-Y. Chen, X.-L. Shi, J. Zou, Z.-G. Chen, Small Methods 6 (2), 2101235 (2022) https://doi.org/10.1002/smtd.202101235.

[107] Z.-G. Chen, W.-D. Liu, Journal of Materials Science & Technology, 121, 2022, 256-262, https://doi.org/10.1016/j.jmst.2021.12.069.

[108] Purdy, D.L. (1986). Nuclear Batteries for Implantable Applications. In: Owens, B.B. (eds) Batteries for Implantable Biomedical Devices. Springer, Boston, MA. https://doi.org/10.1007/978-1-4684-9045-9_11.

[109] Deng H, Nan B, Xu G. Materials. 2023; 16(16):5536. https://doi.org/10.3390/ma16165536.

[110] T. Cao, X.-L. Shi, M. Li, B. Hu, W. Chen, W.-D. Liu, W. Lyu, J. MacLeod, Z.-G. Chen, eScience, 3 (3), 2023, 100122, https://doi.org/10.1016/j.esci.2023.100122.

[111] S. Feng et al. / Computational Materials Science 82 (2014) 45–49. http://dx.doi.org/10.1016/j.commatsci.2013.09.037.

[112] J. O. Jenkins, J. A. Rayne, and R. W. Ure, Phys. Rev. B 5, 3171, 1972. https://doi.org/10.1103/PhysRevB.5.3171.

[113] Bao-Ling Huang and Massoud Kaviany PHYSICAL REVIEW B 77, 125209 2008. https://doi.org/10.1103/PhysRevB.77.125209.

[114] Shrabani Paul, Umapada Pal, Swapan Kumar Pradhan Materials Chemistry and Physics Volume 279, 1 March 2022, 125736 https://doi.org/10.1016/j.matchemphys.2022.125736.

[115] Fei Ren; Hsin Wang; Paul A. Menchhofer; James O. Kiggans Appl. Phys. Lett. 103, 221907 (2013) https://doi.org/10.1063/1.4834700.

[116] Li-Dong Zhao, Bo-Ping Zhang, Jing-Feng Li, Min Zhou, Wei-Shu Liu, Jing Liu Journal of Alloys and Compounds Volume 455, Issues 1–2, 8 May 2008, Pages 259-264 https://doi.org/10.1016/j.jallcom.2007.01.015.

[117] Sejin Byun, Joonil Cha, Chongjian Zhou, Yong Kyu Lee, Hyungseok Lee, Sang Hyun Park, Won Bo Lee, In Chung, Journal of Solid State Chemistry, Volume 269, 2019, Pages 396-400.